Structural insights into a StART-like domain in Lam4 and its interaction with sterol ligands

Alberto T Gatta[a,*,1], Andrea C. Sauerwein[b,*], Anastasia Zhuravleva[c], Tim P Levine[a], Stephen Matthews[b‡]

[a] UCL Institute of Ophthalmology, Department of Cell Biology, 11-43 Bath Street, London EC1V 9EL, UK

[b] Imperial College London, Department of Life Sciences, South Kensington Campus, Exhibition Road, London SW7 2AZ, UK

[c] Astbury Centre for Structural Molecular Biology and Faculty of Biological Sciences, University of Leeds, Leeds LS2 9JT, UK

[1] Present address: Department of Cell Biology, Yale School of Medicine, 333 Cedar St, New Haven, CT 06511, United States.

* These authors contributed equally to this work.

‡ Address for correspondence: s.j.matthews@imperial.ac.uk

Telephone and fax numbers of corresponding author

Authors' email addresses:
ATG, alberto.gatta@yale.edu
ACS, a.sauerwein@imperial.ac.uk
AZ, a.zhuravleva@leeds.ac.uk
TPL, tim.levine@ucl.ac.uk

Abstract

Sterols are essential components of cellular membranes and shape their biophysical properties. The recently discovered family of Lipid transfer proteins Anchored at Membrane contact sites (LAMs) have been suggested to carry out intracellular sterol traffic using StART-like domains. Here, we studied the second StART-like domain of Lam4p from *S. cerevisiae* by NMR. We predicted the structural model of Lam4S2 and we validate it using secondary structure propensities obtained from the NMR analysis of the protein backbone. NMR data revealed enhanced μs-ms flexibility for several functionally important regions, identified the sterol binding site, and suggested the role of membrane interactions on thermodynamics of sterol binding.

Highlights

- An NMR assignment of Lam4S2 identified significant conformational exchange.
- Lam4S2 binding to sterol causes structural changes to the StART-like cavity.
- In a non-membrane environment, the upper limit of sterol exchange is in the 1-10 s^{-1} range.

Keywords

Lipid transfer proteins, Membrane contact sites, Intracellular sterol traffic, Protein-lipid interaction, Nuclear magnetic resonance

Abbreviations

ER, Endoplasmic Reticulum;

LAM, Lipid transfer protein Anchored at a Membrane contact site;

LTP, Lipid Transfer Protein;

NMR, Nuclear Magnetic Resonance.

Introduction

Sterols are essential components of cellular membranes where their concentration determines vital biophysical properties, such as fluidity, rigidity and thickness [1, 2]. Like the majority of lipid molecules, sterols are predominantly made in the endoplasmic reticulum (ER) where they are present at low concentration (5 mol% of lipids). Along the secretory pathway, cholesterol in mammalian cells and ergosterol in fungal cells become enriched in the *trans*-Golgi and plasma membrane, where they account for 30-40 mol% of total lipids [3-5]. The transport of newly synthesised sterols to the plasma membrane is bidirectional and rapid ($t_{1/2}$ <5 min). Furthermore, it is largely independent from vesicular traffic and it is likely to be mediated by soluble sterol Lipid Transfer Proteins (LTPs) [6-9]. Nevertheless, a comprehensive description of the mechanisms of ER to plasma membrane sterol transport is still missing.

We have recently discovered a family of transmembrane proteins that we called Lipid transfer proteins Anchored at Membrane contact sites (LAMs) [10]. Yeast has six LAMs all localised to membrane contact sites between the ER and other organelles. They contain domains that are distant homologues of Steroidogenic Acute lipid Transfer (StART) domains, as identified by HHsearch [11], and these domains have been shown to solubilise [10] and transfer [12] sterols. *S. cerevisiae* contains three paralogous pairs of LAMs, which localise to two places: Lam1/3p and Lam2/4p localise to ER- plasma membrane junctions, while Lam5/6p localise to multiple internal contact sites between the ER and both mitochondria and vacuole [10, 12, 13]. We proposed that Lam1–4p are involved in intracellular sterol traffic between ER and plasma membrane thanks to their predicted StART-like domains [10]. The *in*

vitro ability to transfer sterol was matched by involvement in intracellular sterol traffic *in vivo* [10, 12]. In addition, action of LAM domains in creating resistance in yeast to the antifungal drug Amphotericin B domains suggested that the domains of Lam2/4/5/6p and the human LAMs all bind sterol [10].

The ability to solubilise lipids into aqueous solution is a general property of StART-like domains. They have a characteristic β-grip fold that forms a deep hydrophobic pocket capable of harbouring a lipid. The minimal StART-like domain consists of ~170 aa forming a seven stranded curved β-sheet that curves round ("grips") one long helix and 2 short helices. Many StART-like families can be grouped together by structural and remote sequence homology into a large StAR-kin superfamily. Like other superfamilies, these relationships are discoverable not through primary structure alone, but require three-dimensional alignment [14]. The β-grip has an internal cavity between the helices and the sheet with a typical volume 400-700Å^3, which allows one lipid to bind inside [15]. There is as yet no structural evidence to support the structural predictions made for the StART-like domains in LAMs. Here, we used solution NMR to probe the structural and dynamic features of the second StART-like domain of Lam4p (Lam4S2) in its apo- and holo- states.

Materials and methods

Protein expression and purification

Lam4S2 (235 residues, sequence MGGSHHHHHHGMASHHHHHHARAM + Lam4 residues 946-1155 + DV-stop) was produced as previously described [10], with some modifications for isotope labelling [16]. A single colony of BL21(DE3) cells transformed with pTrcHis$_{11}$-Lam4S2 was grown overnight at 30°C in LB medium. The culture was diluted into unlabelled M9 medium (45 mM Na_2HPO_4, 20 mM KH_2PO_4, 10 mM NaCl, 1 mM $MgSO_4$, 0.1 mM $CaCl_2$, 20 mM NH_4Cl) + 2.5% LB at 37°C. At OD_{600} ~0.5 the culture was diluted 1:120,000 in 100 ml of unlabelled M9 medium + 2.5% LB and left overnight at 30°C. Log-phase growing cells were resuspended in 500 ml of labelled M9 medium made with 45 mM Na_2HPO_4, 20 mM KH_2PO_4, 10 mM NaCl, 1 mM $MgSO_4$, 0.1 mM $CaCl_2$, 20mM $^{15}NH_4Cl$ (Goss Scientific, Cat. No. NLM467) + 2.5% LB and transferred at 37°C. At OD_{600} = 0.5 the culture is diluted in 2 litres of labelled M9 medium + 2.5% LB. Protein overexpression was induced at OD_{600} = 0.5 with 0.2 mM IPTG for 6 hours at 37°C. Cells were lysed in lysis buffer: 25 mM Tris-HCl pH 8.0, 300 mM NaCl, 10 mM imidazole, 0.5 mM DTT, 1 cOmplete EDTA-free protease inhibitor cocktail tablet (Roche, Cat.no. 11873580001), 0.1 mg/ml lysozyme chloride form. The protein was purified following the previously published protocol [10], but desalted into a buffer optimised for NMR: 10 mM PIPES pH 6.8, 50 mM L-Arginine (Sigma, Cat.no. A5006), 50 mM L-Glutamate (Sigma, Cat.no. G1626), 49 mM NaCl, 1 mM KCl [17].

Double labelled Lam4S2 samples (^{13}C, ^{15}N) were grown according to the above protocol in presence of both 20 mM $^{15}NH_4Cl$ and 10 mM D-[^{13}C]-glucose (Goss Scientific, Cat. No. CLM1396). Triple labelled Lam4S2 samples (^{2}H, ^{13}C, ^{15}N) were

grown in $^{2}H_2O$ according to the above protocol in presence of both 20 mM $^{15}NH_4Cl$ and 10 mM D-[^{13}C]-glucose (Goss Scientific, Cat. No. CLM1396). This followed a $^{2}H_2O$-adaptation of BL21(DE3) *E. coli* colonies which were selected from a $^{2}H_2O$-based M9 minimal medium agar plate grown for 2 days at 37 °C.

Backbone chemical shift assignment

Assignment experiments for Lam4S2 were carried out at protein concentrations from 0.35 to 0.5 mM in the following NMR buffer: 10 mM PIPES pH 6.8, 50 mM L-Arg + L-Glu pH 6.8, 49 mM NaCl, 1 mM KCl, 10 % $^{2}H_2O$. On the ^{1}H-^{13}C-^{15}N sample HNCA, HNCACB, HN(CA)CO, HNCO and HN(CO)CA [18] BEST-TROSY experiments were recorded at 288 K, 293 K, 298 K and 303 K (15°C to 30°C) using Bruker Avance II 600 MHz, equipped with the TCI cryogenically cooled probe (MRC Biomedical NMR Centre, Mill Hill, London), a Varian INOVA 600 MHz magnet (Faculty of Biological Sciences, University of Leeds), and Bruker Avance II 900 MHz, equipped with the TCI cryogenically cooled probe (Biomolecular NMR facility, University of Birmingham). Assignment experiments on the triple labelled ^{2}H-, ^{13}C-, ^{15}N-Lam4S2 sample were carried out at 283 K on a Bruker DRX800 spectrometer equipped with a cryo-probe (Cross Faculty NMR Centre, Imperial College London). These experiments were recorded in their TROSY implementations for use with backbone chemical shift assignments: HNCO, HN(CO)CA, HNCACB, HN(CA)CO, HN(CO)CACB and HNCA. Data were processed using NMRpipe [19].

Backbone assignment of Lam4S2 was initially performed semi-automatically using MARS [20], then subsequently confirmed and completed manually.

Chemical shift analysis and homology modelling

To gain structural information from the backbone chemical shift assignment of LAM4S2 the assigned chemical shifts were used with TALOS-N [21] which predicted secondary structure elements from the observed experimental shifts. The secondary structure calculation from TALOS-N was used as the secondary structure input for i-Tasser [22-24] to obtain a Lam4S2 model.

Cholesterol titrations and line shape analysis

Two 140 µM ^{2}H-, ^{13}C-, ^{15}N-Lam4S2 samples were titrated with either the sterol ligand or a control. The ligand is a preparation of 6 mM cholesterol : 30 mM methyl β-cyclodextrin (MβCD) [25], while the control sample contains only 30 mM MβCD. The protein samples, and both additives are dissolved in the same NMR buffer: 10 mM PIPES pH 6.8, 50 mM L-Arg + L-Glu pH 6.8, 49 mM NaCl, 1 mM KCl, 10 % $^{2}H_2O$, Both samples were titrated at protein:cholesterol ratios of 1:0, 1:0.25, 1:0.5, 1:0.75, 1:1, 1:2 and 1:4. ^{1}H-, ^{15}N-TROSY-HSQC spectra were recorded at each data point at 283K on a Bruker DRX800 spectrometer equipped with a cryo-probe Titration data were processed with exponential line broadening using nmrPipe [19] then imported into TITAN [26] for line shape analysis. Data were fitted to a two-state ligand binding model in a two-stage process: chemical shifts and linewidths of the free state were determined using the first spectrum only, then chemical shifts of the bound state, linewidths of all states, and the binding model parameters K_d and k_{off} were fitted using the entire dataset.

Results and discussion

Lam4S2 NMR fingerprint

The ^{1}H, ^{15}N HSQC-TROSY of Lam4S2 (Figure 1) shows the NMR fingerprint of the protein recorded after optimising the buffer conditions for NMR from those optimal for *in vitro* binding assays [10] to a lower salt buffer that contains 50 mM L-Arginine/L-Glutamate solution to improve signal-to-noise ratio and increase protein solubility [17]. The ^{1}H, ^{15}N HSQC-TROSY of Lam4S2 (Figure 1) contains 204 backbone amide peaks. This corresponds to 92% of the 222 peaks, which are expected to be observable from the 235 residue LAM2S2 construct. The chemical shift dispersion indicates a folded protein, and the absence of multiple peaks for a single backbone amide suggested a single conformation. The intense peaks detected at proton chemical shifts of ~8 ppm are probably part of the unfolded 11-histidine tag. Additionally to the backbone amides, two tryptophan amine resonances are observed at proton chemical shifts of 10.5 and 11.2 ppm.

Lam4S2 backbone assignment

The backbone assignment of Lam4S2 is based on double- and triple-labelled samples of Lam4S2. Analysis of the initial data recorded on the double-labelled sample (^{15}N-^{13}C-Lam4S2) could assign only 50% of the residues because the low quality of the triple resonance spectra (particularly, HNCACB and HN(CA)CO experiments) was not enough to obtain the unambiguous backbone assignments. The lack of signal in triple resonance spectra of the protonated sample is due, in part, to the relatively large size of the polypeptide (MW = 26.5 kDa). This led us to adopt an assignment strategy employing deuteration to improve the relaxation

properties of the sample and improve the sensitivity of the assignment experiments. Furthermore, spectral resolution and sensitivity were improved by working at a higher magnetic field (18.8 T instead of 14.1 T) and recording the experiments using TROSY-based triple resonance experiments.

Fractional deuteration (~75%) of Lam4S2 increased the number of peaks observed in the triple resonance experiments Significant line broadening was observed for a number of peaks in 2D and 3D spectra, apparently suggesting that some parts of the protein involved into a μs-ms exchange process, that significantly complicate the assignments. Finally, a combination of triple resonance experiments recorded for non-deuterated and deuterated proteins at several magnetic fields and temperatures allowed backbone assignments for ~54% protein construct (Fig. 2A, B). This partial assignment (Figure 1) covers 70% of the pseudo-residues observed but only 54% of the protein construct. Figures 2A and 2B illustrate the parts of Lam4S2 we assigned, and they identify the regions for which we did not obtain an assignment. It is apparent that the unstructured loops of the protein where readily assigned while the core residues of the β-sheets (β1, β3, β4, β5, β6, and β7) forming the hydrophobic cavity are largely unassigned due to missing chemical shift data in either the 3D experiments or the 2D and 3D experiments.

These observations are likely due to conformational exchange on a millisecond to microsecond timescale. Notably, β6 a central strand within the β-sheet) contains a contiguous hydrophobic stretch of amino acids 'IFLFW' (1082-1086) that is unassigned (blue patch in Fig. 2B). In the predicted structure, the two phenylalanines are solvent exposed and flanked by additional hydrophobic residues exposed on neighbouring strands. We suggest that this may be an interaction site for a separate

domain. In the absence of its binding partner, this segment could contribute to self-association, which would introduce the exchange broadening observed in the NMR spectrum. Interestingly, both Lam2p and Lam4p possess two conserved StART-like domains in their sequence, which may interact with each other via this surface and function in a co-regulatory role.

The resulting partial chemical shift assignment of Lam4S2 is not sufficient for *de novo* structural calculations. Therefore, we employed homology modelling restrained by the chemical shift based secondary structure prediction of TALOS-N to obtain a structural model of Lam4S2 (Figure 2).

Residues affected by sterol binding

The available backbone assignment of Lam4S2 was used to determine the role of the assigned residues in sterol binding. Titration of a MβCD:sterol complex into a Lam4S2 protein sample resulted in the decrease of peak intensities of a small set of apo peaks, while additional cholesterol-bound peaks appeared at different distinct sets of chemical shifts. NMR data are shown in Figure 3A for selected peaks. The cholesterol-bound peaks increased in intensity with increasing cholesterol concentrations. These results suggest that the cholesterol:Lam4S2 complex is in slow exchange on the NMR chemical shift timescale. The control set of titrations of MβCD with LAM4S2 showed no changes in chemical shifts (data not shown) confirming that the observed chemical shift changes are indeed due to cholesterol binding.

Cholesterol titration experiments allowed us to identify the residues involved in sterol binding as being in the N-terminal loop (S954, A956, D965), β1 (I971 and E973), α2 (T993 and E994), β2 (E1010), and others in the loops between the antiparallel β-sheets (S1018, T1067, G1073, and H1089). Additional to those residues identified via their backbone amide chemical shifts it was striking that one of the tryptophan side chain amines showed chemical shift changes upon cholesterol binding, while the other tryptophan did not display any changes in chemical shift. Considering the structural information on Lam4S2, W1086 was predicted to face outside the binding pocket, while W1102 was predicted to face inside the binding pocket [10]. So this is very likely to be the residue showing the significant chemical shift.

A more quantitative titration of the Lam4S2 cholesterol was conducted to obtain kinetic parameters of the cholesterol binding. Analysis was conducted by quantum mechanical simulation of the titration data and subsequent fitting of the 2D experiment to allow a quantitative analysis of the resonance lineshape [26]. The experimental data and the simulated data for selected peaks are shown in Figure 3A. When selecting a peak for lineshape analysis a region of interest and the peak position are chosen in all spectra, and this input is used to fit the lineshape of all selected peaks. Examples of peak fitting are provided in Supplementary Figures 1 and 2. Data are then fitted to a two-state ligand-binding model in a two-stage process. First, the chemical shifts and the linewidth of the free (protein only) state were determined. Second, those parameters were used with the chemical shift of the cholesterol bound state and the linewidths of all states to fit the parameters K_d and k_{off} to the entire dataset (Figure 3B). The K_d obtained was 140 μM. This is 2 orders of magnitude higher than the dissociation constant measured when the same domain

was presented with sterol in liposome bilayers (K_d = 0.5 μM) [10]. This large difference might be explained by structural analysis of other StART domains. StARD4 undergoes conformational changes in the C-terminal helix and the Ω-loop when it interacts with a bilayer [27]. These changes expose the internal cavity and allow lipid entry/exit. If LAMs have a similar opening mechanism, cyclodextrins would be very poor donors since they do not mimic a membrane, so the entry site of the domain would not be held open. From the K_d it was possible to estimate a k_{off} of about 6 molecules per second. This value falls in an acceptable range if compared with the rate of transfer of other StART domains [27], and once the sterol molecule is bound in the hydrophobic pocket, the role of membrane interaction could be less relevant for lipid unloading. However, the clear message is that specific residues in Lam4S2 are affected by the addition of cholesterol and hence involved in sterol binding: part of the long helix (α_3), residues along α_2 and the Ω-loop contacting α_3, and the assigned tryptophan (W1102).

In summary we can say that the chemical shift information obtained during the assignment of Lam4S2 has allowed us to present a refined homology model. This model is consistent with sterol binding inside an internal hydrophobic cavity, and therefore with the domain assuming the StART-like fold predicted for it by bioinformatics approaches [10, 28]. Furthermore, structural changes upon specific sterol binding could be observed. Any further studies that would allow a more in depth characterisation of the sterol binding need to address the conformational exchange due to domain association — ideally by working in the natural context of the twin StART-like domains.

Acknowledgements

This work was supported by funds from Medical Research Council and by a Senior Investigator award from the Wellcome Trust to SM; by the Marie-Curie ITN 'Sphingonet' (European Commission FP7, grant no. 289278) to ATG, TPL. We thank Dr Alain Oregioni (MRC Biomedical NMR Centre, The Francis Crick Institute, London, U.K.), and Dr Sara Whittaker (HWB-NMR, University of Birmingham) for assistance with NMR data collection.

Figure/Table Legends

Figure 1.

Lam4S2 assignment. Partially assigned ^{1}H, ^{15}N–HSQC-TROSY spectrum of the recombinant ^{2}H, ^{13}C, ^{15}N-Lam4S2 domain. The peaks are labelled using the single letter amino acid code followed by their position in the recombinant Lam4S2 construct.

Figure 2.

Secondary structure determination using TALOS-N and comparison to Lam4S2 homology model. (A) Distribution of assigned peaks over the Lam4S2 sequence. Blue bars represent where an assignment is available; elsewhere experimental data are missing. (B) Homology model of Lam4S2. Highlighted in green are the residues for which experimental data in the form of a chemical shift assignment are available; highlighted in blue is the unassigned hydrophobic patch potentially involved in domain-domain interaction. (C) The predicted secondary structure of Lam4S2 using TALOS N and the available chemical shift data. The Lam4S2 sequence is predicted to consist of 3 α-helices and 7 β-strands. Helices are located between residues 59-65, 67-80, 182-217 with a kink at residues 191/192, similar to that seen in both PCTP and StARD5 (1LN1 and 2R55 respectively), β-strands are located between residues 48-51, 88-90, 102-109, 122-124, 136-141, 155-164 and 171-179. (D) Lam4S2 StART-like domain with detailed secondary structure elements as obtained by prediction and verified by NMR chemical shifts. Residues involved in sterol binding (annotated balls), including W1102 (sticks), and the residues in the Ω-loop contacting α_3 are mapped on the model.

Figure 3.

Analysis of the Lam4S2 interaction with cholesterol. (A) Observed and fitted ^{1}H, ^{15}N-HSQC-TROSY spectra of 140 μM ^{2}H-^{13}C-^{15}N-Lam4S2 upon titration of MβCD:cholesterol for selected peaks included in the global fit of binding model parameters. (B) Binding model parameters for the interaction of Lam4S2 with cholesterol.

Figures/Tables

Figure 1.

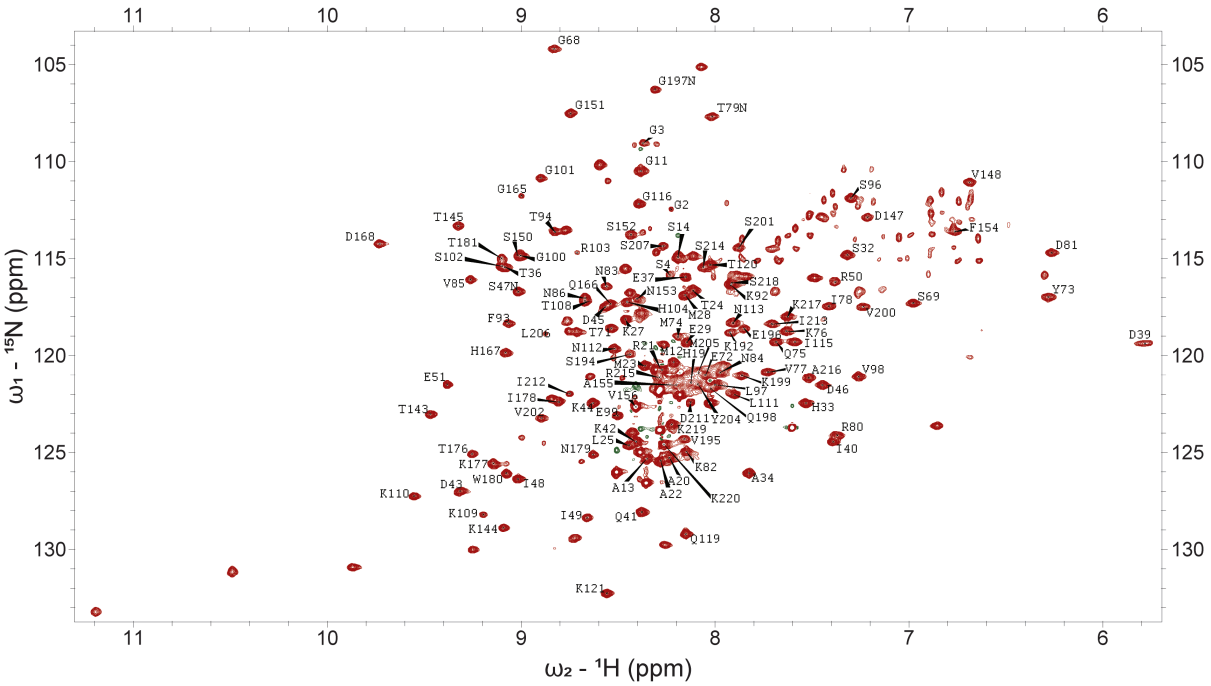

Figure 2.

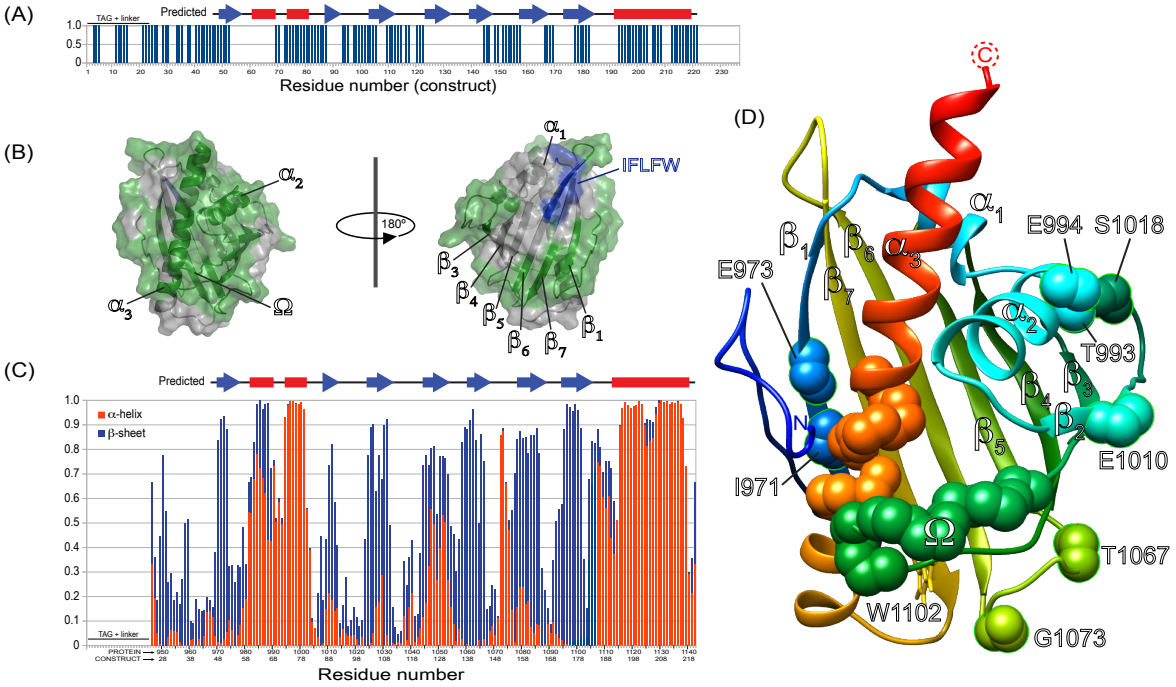
(A)
Predicted
TAG + linker
Residue number (construct)
(B)
IFLFW
180°
(C)
Predicted
α-helix
β-sheet
TAG + linker
Residue number
(D)
E994
S1018
E973
T993
E1010
I971
T1067
W1102
G1073
N
C

Figure 3.

(A)

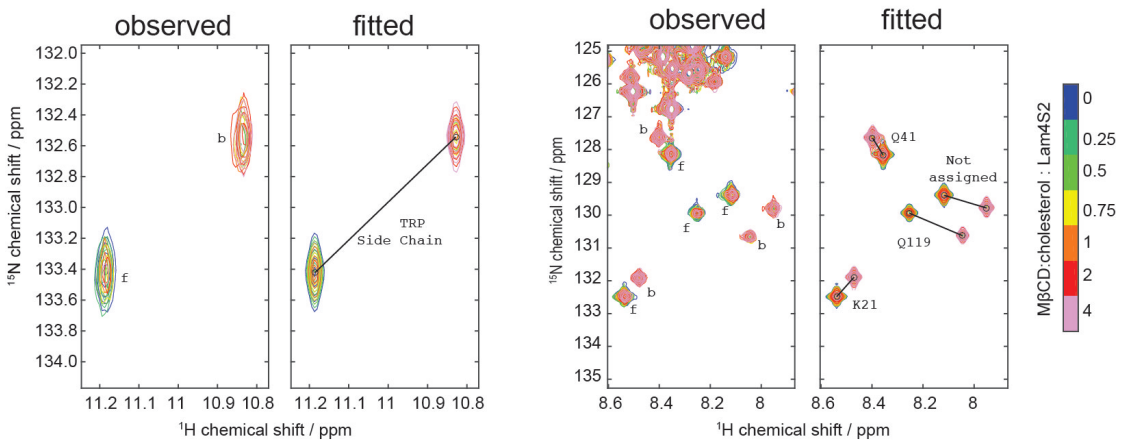

(B)

	fitted $\mathbf{k_d}$ (μM)	fitted $\mathbf{k_{off}}$ (s^{-1})
MβCD:cholesterol	141.5 ± 1.2	6.2 ± 0.1

Supplementary Material

Supplementary Figure 1.

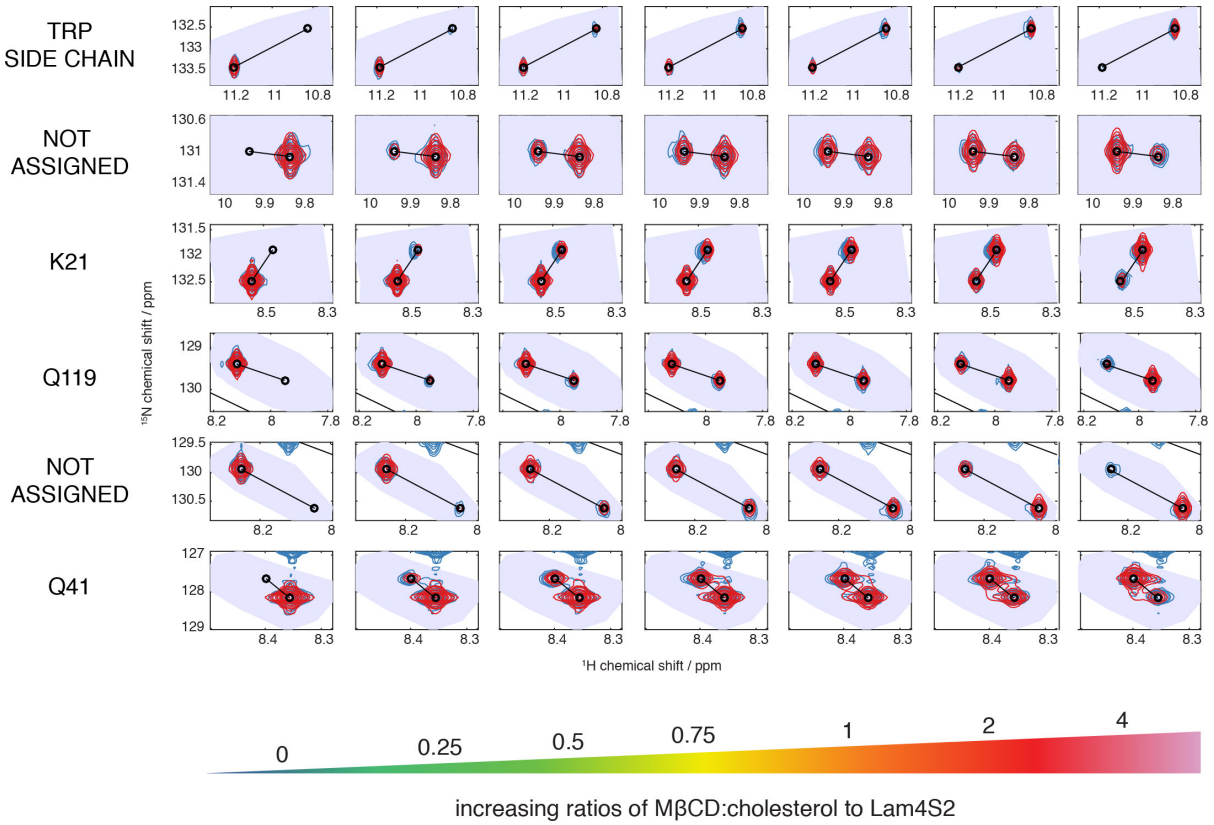

Line shape analysis using TITAN. Grid view off all fits used to calculate the cholesterol binding kinetics to Lam4S2. From left to right: the Lam4S2-to-cholesterol ratio increases from 1:0 to 1:4. Fits are shown as contour plot.

Supplementary Figure 2.

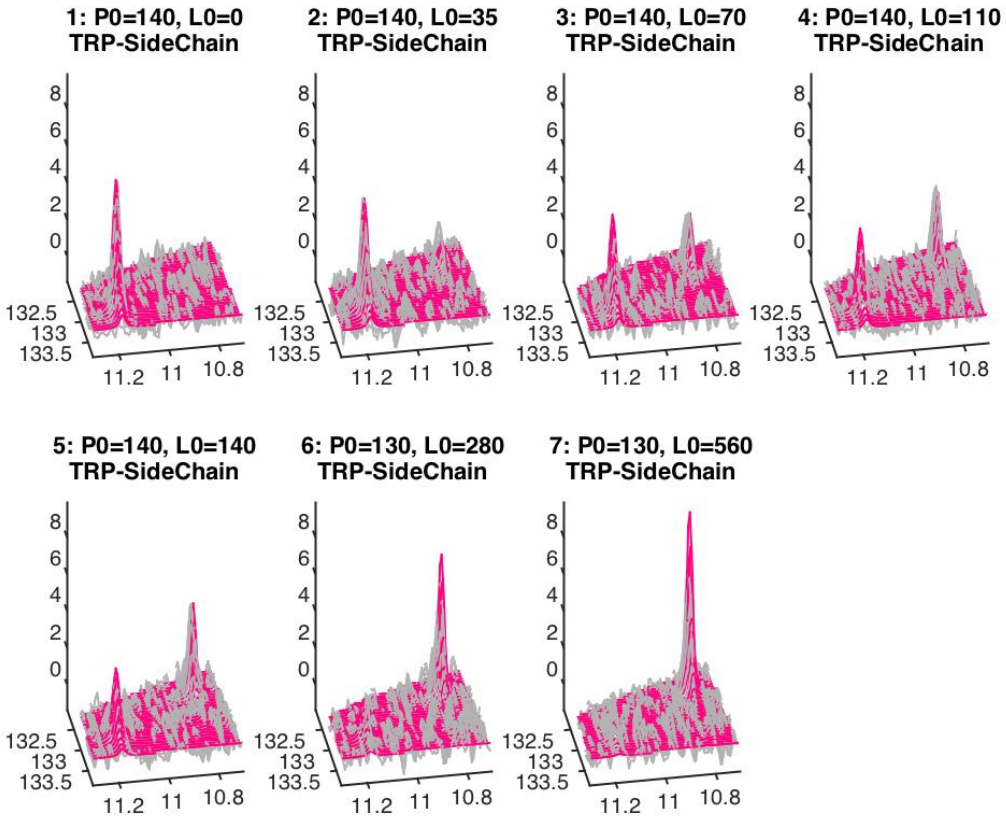

3D line shape fits obtained by TITAN. The experimental data (grey) — here for a TRP side chain residue — are overlaid with the simulated data (red), which were obtained using TITAN during the calculation of the cholesterol binding kinetics.

References

1. Holthuis, J.C. and A.K. Menon, *Lipid landscapes and pipelines in membrane homeostasis.* Nature, 2014. **510**(7503): p. 48-57.
2. van Meer, G., D.R. Voelker, and G.W. Feigenson, *Membrane lipids: where they are and how they behave.* Nature reviews. Molecular cell biology, 2008. **9**: p. 112-124.
3. Orci, L., et al., *Microheterogeneity of protein and sterol content in kidney podocyte membrane.* Nature, 1981. **293**: p. 646-647.
4. Simons, K. and E. Ikonen, *How cells handle cholesterol.* Science (New York, N.Y.), 2000. **290**: p. 1721-1726.
5. Radhakrishnan, A., et al., *Switch-like control of SREBP-2 transport triggered by small changes in ER cholesterol: a delicate balance.* Cell metabolism, 2008. **8**: p. 512-521.
6. Urbani, L. and R.D. Simoni, *Cholesterol and vesicular stomatitis virus G protein take separate routes from the endoplasmic reticulum to the plasma membrane.* The Journal of biological chemistry, 1990. **265**: p. 1919-1923.
7. DeGrella, R.F. and R.D. Simoni, *Intracellular transport of cholesterol to the plasma membrane.* The Journal of biological chemistry, 1982. **257**: p. 14256-14262.
8. Field, F.J., et al., *Transport of cholesterol from the endoplasmic reticulum to the plasma membrane is constitutive in CaCo-2 cells and differs from the transport of plasma membrane cholesterol to the endoplasmic reticulum.* The Journal of Lipid Research, 1998. **39**: p. 333-343.
9. Baumann, N.A., et al., *Transport of Newly Synthesized Sterol to the Sterol-Enriched Plasma Membrane Occurs via Nonvesicular Equilibration †.* Biochemistry, 2005. **44**: p. 5816-5826.
10. Gatta, A.T., et al., *A new family of StART domain proteins at membrane contact sites has a role in ER-PM sterol transport.* eLife, 2015. **4**: p. 1-46.
11. Soding, J., A. Biegert, and A.N. Lupas, *The HHpred interactive server for protein homology detection and structure prediction.* Nucleic Acids Res, 2005. **33**(Web Server issue): p. W244-8.
12. Murley, A., et al., *Ltc1 is an ER-localized sterol transporter and a component of ER-mitochondria and ER-vacuole contacts.* The Journal of Cell Biology, 2015. **209**: p. 539-548.
13. Elbaz-Alon, Y., et al., *Lam6 Regulates the Extent of Contacts between Organelles.* Cell reports, 2015. **12**: p. 7-14.
14. Wong, L.H. and T.P. Levine, *Lipid transfer proteins do their thing anchored at membrane contact sites… but what is their thing?* Biochem Soc Trans, 2016. **44**: p. 517–527.
15. Schrick, K., et al., *Shared functions of plant and mammalian StAR-related lipid transfer (START) domains in modulating transcription factor activity.* BMC Biol, 2014. **12**: p. 70.
16. Tugarinov, V., V. Kanelis, and L.E. Kay, *Isotope labeling strategies for the study of high-molecular-weight proteins by solution NMR spectroscopy.* Nature Protocols, 2006. **1**: p. 749-754.

17. Golovanov, A.P., et al., *A Simple Method for Improving Protein Solubility and Long-Term Stability.* Journal of the American Chemical Society, 2004. **126**: p. 8933-8939.
18. Ikura, M., L.E. Kay, and A. Bax, *A novel approach for sequential assignment of 1H, 13C, and 15N spectra of proteins: heteronuclear triple-resonance three-dimensional NMR spectroscopy. Application to calmodulin.* Biochemistry, 1990. **29**: p. 4659-4667.
19. Delaglio, F., et al., *NMRPipe: a multidimensional spectral processing system based on UNIX pipes.* J Biomol NMR, 1995. **6**(3): p. 277-93.
20. Jung, Y.S. and M. Zweckstetter, *Mars -- robust automatic backbone assignment of proteins.* J Biomol NMR, 2004. **30**(1): p. 11-23.
21. Shen, Y. and A. Bax, *Protein backbone and sidechain torsion angles predicted from NMR chemical shifts using artificial neural networks.* J Biomol NMR, 2013. **56**(3): p. 227-41.
22. Zhang, Y., *I-TASSER server for protein 3D structure prediction.* BMC Bioinformatics, 2008. **9**: p. 40.
23. Roy, A., A. Kucukural, and Y. Zhang, *I-TASSER: a unified platform for automated protein structure and function prediction.* Nature Protocols, 2010. **5**: p. 725-738.
24. Yang, J., et al., *The I-TASSER Suite: protein structure and function prediction.* Nat Methods, 2015. **12**(1): p. 7-8.
25. Maxfield, F.R. and D. Wüstner, *Analysis of Cholesterol Trafficking with Fluorescent Probes BT - (null)*, in *Methods in Cell Biology*. 2012, Elsevier. p. 367-393.
26. Waudby, C.A., et al., *Two-Dimensional NMR Lineshape Analysis.* Sci Rep, 2016. **6**: p. 24826.
27. Iaea, D.B., et al., *STARD4 Membrane Interactions and Sterol Binding.* Biochemistry, 2015. **54**(30): p. 4623-36.
28. Khafif, M., et al., *Identification and phylogenetic analyses of VASt, an uncharacterized protein domain associated with lipid-binding domains in Eukaryotes.* BMC Bioinformatics, 2014. **15**: p. 222.